

See discussions, stats, and author profiles for this publication at: <https://www.researchgate.net/publication/237331425>

# Effect of co-sensitization in new hybrid photo-refractive materials based on PVK polymer matrix and inorganic LiNbO<sub>3</sub> nano-crystals

Article in Applied Physics B · June 2009

DOI: 10.1007/s00340-009-3544-6

CITATIONS

8

READS

36

5 authors, including:



Ewa A. Sliwinska

University of Cologne

17 PUBLICATIONS 75 CITATIONS

[SEE PROFILE](#)



Mansurova Svetlana

Instituto Nacional de Astrofísica, Óptica y Electrónica (INAOE)

58 PUBLICATIONS 214 CITATIONS

[SEE PROFILE](#)



Karsten Buse

University of Freiburg

362 PUBLICATIONS 6,244 CITATIONS

[SEE PROFILE](#)



Klaus Meerholz

University of Cologne

350 PUBLICATIONS 13,267 CITATIONS

[SEE PROFILE](#)

Some of the authors of this publication are also working on these related projects:



University of Cologne [View project](#)



Optical characterization methods [View project](#)

# Effect of co-sensitization in new hybrid photo-refractive materials based on PVK polymer matrix and inorganic LiNbO<sub>3</sub> nano-crystals

E. Śliwińska · S. Mansurova · U. Hartwig · K. Buse · K. Meerholz

Received: 20 February 2009 / Revised version: 29 March 2009 / Published online: 2 May 2009  
© Springer-Verlag 2009

**Abstract** A new class of photo-refractive (PR) composite materials based on poly(*N*-vinylcarbazole) (PVK) (co-) sensitized with nano-crystalline lithium niobate (LiNbO<sub>3</sub>) is presented. The steady-state performance, as well as the kinetics of the photo-refractive grating formation, was investigated by degenerate four-wave mixing (DFWM) and two-beam-coupling (TBC) experiments. We found an optimum content of LiNbO<sub>3</sub> nano-particles of only 10<sup>-3</sup> wt.%. Even at concentrations as low as 10<sup>-7</sup> wt.% a notable effect of the nano-crystals was detected. This yields materials with improved PR performance compared to that of the standard PR polymer material sensitized by TNF only. The role of LiNbO<sub>3</sub> nano-particles is discussed in detail: The particles support generation and transport of the free-charge carriers. Furthermore, they increase the electron trap density.

**PACS** 77.84.Nh · 78.67.Bf · 81.07.-b

## 1 Introduction

The photo-refractive (PR) effect, discovered in 1966 in LiNbO<sub>3</sub> [1], is considered today to be one of the most

promising mechanisms for many potential holographic applications, including real-time image processing, phase conjugation, and selective laser feedback, because the writing process is reversible and requires only low light intensities [2]. In a PR material holograms can be stored as modulations of the refractive index using light sources of relatively low power (e.g., laser diodes). In 1991, the PR effect was observed for the first time in a polymer [3]. This discovery initiated intense research efforts. Following various design concepts, a huge number of new PR polymers has been developed and their PR properties improved rapidly [4–8].

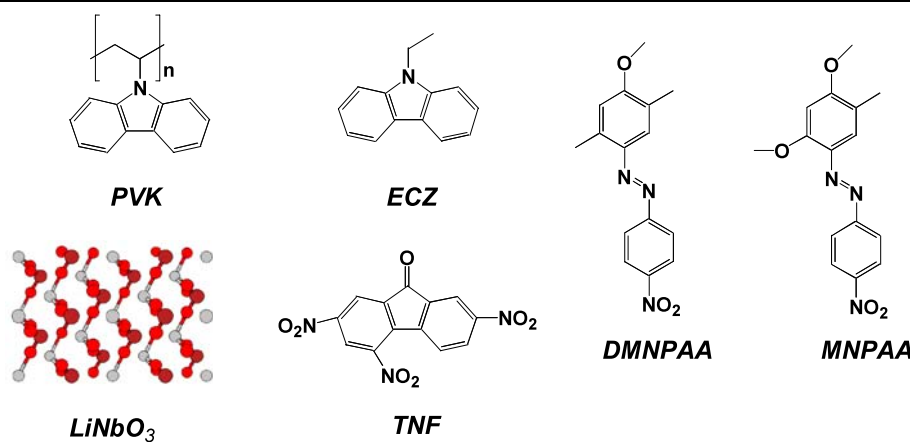
One class of PR materials are the hybrid composites consisting of inorganic nano-particles embedded into a polymer matrix [9–11]. This contribution reports on a novel class of PR materials combining the most studied organic and inorganic PR systems. They consist of lithium niobate (LiNbO<sub>3</sub>) nano-particles (NP) embedded into an amorphous PR polymer composite derived from the first high-performance PR polymer based on the photo-conductor poly(*N*-vinylcarbazole) (PVK) [4, 12]. We expect that the nano-crystal/polymer hybrid materials offer additional advantages over the existing photo-refractive materials, e.g., a faster response, a broad-band spectral sensitivity, and new photo-refractive properties. In a previous study we incorporated LiNbO<sub>3</sub> NP into PVK and found that the drift length of free holes is enlarged due to trapping of electrons by the LiNbO<sub>3</sub> nano-particles and therefore increased recombination time of the free holes [13]. These results encouraged us to employ the LiNbO<sub>3</sub> NP also in a PR hybrid material that also contains—in addition to the material studied in Ref. [13]—electro-optic chromophores.

E. Śliwińska · K. Meerholz (✉)  
Chemistry Department, University of Cologne,  
Luxemburger Str. 116, 50939 Cologne, Germany  
e-mail: klaus.meerholz@uni-koeln.de

S. Mansurova  
National Institute for Astrophysics, Optics and Electronics,  
AP 51 y 216, Puebla 72000, Mexico

U. Hartwig · K. Buse  
Institute of Physics, University of Bonn, Wegelerstr. 8,  
53115 Bonn, Germany

**Fig. 1** Chemical structures of the compounds used in this study



## 2 Experimental methods

The components of the composite materials studied in this paper contained the photo-conductor PVK, the plasticizer *N*-ethylcarbazole (ECZ), the chromophores 2,5-dimethyl-4-*p*-nitrophenylazoanisole (DMNPAA) and 3-methoxy-4-*p*-nitrophenylazoanisole (MNPAA), the sensitizers 2,4,7-trinitro-9-fluorenone (TNF), and LiNbO<sub>3</sub> NP. The chemical structures of the compounds are depicted in Fig. 1. PVK and ECZ were purchased from Aldrich, the DMNPAA and MNPAA were synthesized by standard azo coupling of the appropriate subunits. The LiNbO<sub>3</sub> NP was prepared by following a procedure published earlier [14]. The size of the NP was about 20 nm in diameter.

For mixing, all components were dissolved in dichloromethane, and the solvent was then allowed to evaporate. Uniform films were fabricated by sandwiching the composite between two transparent indium–tin–oxide-coated glass substrates at elevated temperature using glass spacer beads to adjust the film thickness to  $d = 105 \mu\text{m}$ . All devices, also those containing NP's, exhibited excellent optical quality.

Two series of materials were prepared (Table 1): In the first series (A–I), the concentration of the standard sensitizer TNF was 1 wt.% and different amounts of LiNbO<sub>3</sub> NPs (from  $10^{-7}$  to 2 wt.%) were added. The reference material R did not contain LiNbO<sub>3</sub>. In the second series (A'–I'), the content of LiNbO<sub>3</sub> was again varied (from  $10^{-7}$  to 2 wt.%), however, in the absence of TNF. The reference material R' did neither contain LiNbO<sub>3</sub> nor TNF.

Materials with low contents of LiNbO<sub>3</sub> (from  $10^{-7}$  to  $10^{-3}$  wt.%) were prepared by diluting the composite with higher content by 1:100, while the higher amounts of LiNbO<sub>3</sub> (from  $10^{-1}$  to 2 wt.%) were directly added to the composite. The glass-transition temperature  $T_g$  was investigated by differential scanning calorimetry in selected cases (heating rate of  $10 \text{ K min}^{-1}$ ). The obtained  $T_g$  started from  $16^\circ\text{C}$  in the absence of NP (materials A and A') and was slightly lowered by the presence of the NP, reaching  $13^\circ\text{C}$

**Table 1** The sensitizer contents in the investigated materials (wt.%) are listed. The other components were 41.5 wt.% PVK, 7.5 wt.% ECZ, 25 wt.% DMNPAA, and 25 wt.% MNPAA, respectively. Furthermore, the glass-transition temperatures ( $T_g$ ) measured by DSC are listed

Composites	Sensitizers		$T_g/^\circ\text{C}$
	TNF	LiNbO <sub>3</sub>	
R	1.0	0	16
A	1.0	$10^{-7}$	
B	1.0	$10^{-5}$	
C	1.0	$10^{-3}$	15
D	1.0	0.1	
E	1.0	0.2	
F	1.0	0.5	
G	1.0	1.0	
H	1.0	1.5	
I	1.0	2.0	13
R'	0	0	16
A'	0	$10^{-7}$	
B'	0	$10^{-5}$	
C'	0	$10^{-3}$	
D'	0	0.1	
E'	0	0.2	
F'	0	0.5	14
G'	0	1.0	
H'	0	1.5	
I'	0	2.0	13

for materials I and I' with the maximum amount of NP (Table 1). Samples with LiNbO<sub>3</sub> NP particle contents exceeding 2 wt.% showed clearly light scattering, samples with NP concentrations below 1 wt.% exhibited no scattering at all.

The photo-conductive properties of the composites were studied by a modulated photo-current technique. In these experiments the DC-biased sample was homogeneously illuminated by HeNe laser light ( $\lambda_0 = 632.8 \text{ nm}$ ) whose inten-

sity was periodically varied with the frequency  $\Omega = 10$  Hz. A time modulated photo-conductivity is created and application of an external electric field yields the modulated photocurrent. The photo-current was detected by an SRS 830 lock-in amplifier with  $R_L = 10\text{ M}\Omega$  input resistance.

The PR properties were investigated at  $T = 21^\circ\text{C}$  by degenerate four-wave mixing (DFWM) and two-beam-coupling (TBC) experiments in a tilted geometry (tilt angle  $\psi_{\text{ext}} = 60^\circ$ ) using a HeNe laser. The writing beams (1 and 2, respectively) were s-polarized, the external beam angles were  $\alpha_{1,\text{ext}} = 50^\circ$  and  $\alpha_{2,\text{ext}} = 70^\circ$ , and the external intensities were  $I_{1,\text{ext}} = 340\text{ mW cm}^{-2}$  and  $I_{2,\text{ext}} = 930\text{ mW cm}^{-2}$ , respectively. Considering the reflection losses, this ensures equal internal intensities (grating contrast  $m \approx 1$ ). The recorded grating was read by an independent weak p-polarized reading beam ( $I_{R,\text{ext}} = 3\text{ mW cm}^{-2}$ ) [4].

The internal diffraction efficiency  $\eta_{\text{int}}$  is defined as the ratio between the intensity of the diffracted light and the overall light intensity behind the sample, i.e., the sum of the intensities of the diffracted and transmitted beams,  $I_{R,\text{diff}}$  and  $I_{R,\text{trans}}$ , respectively [15]:

$$\eta_{\text{int}} = \frac{I_{R,\text{diff}}}{I_{R,\text{diff}} + I_{R,\text{trans}}}. \quad (1)$$

According to the coupled-wave theory [16],  $\eta_{\text{int}}$  can be approximated by

$$\eta_{\text{int}} = \sin^2(\nu) \quad \text{with } \nu = C_{\text{DFWM}} \Delta n, \quad (2)$$

where  $C_{\text{DFWM}} = \pi d / [\lambda_0 \cos(\alpha_{1,\text{int}})]$  is a constant that contains, among other things, the thickness of the sample  $d$ , the angle of incidence of the probe beam  $\alpha_{1,\text{int}}$  inside the sample, and the probe-beam vacuum wavelength  $\lambda_0$ . Here  $\Delta n$  is the index modulation amplitude of the recorded hologram.

Generally, for organic PR materials, in DFWM experiments the diffraction efficiency  $\eta_{\text{int}}$  increases with increasing external field and reaches a maximum for a specific field value  $E_{(\eta_{\text{max}})}$  [4, 12]. This means that the argument  $\nu$  of the function describing the diffraction efficiency (Eq. 2) becomes  $\nu = \pi/2$ . Since the recording geometry is identical in all cases, the index modulation amplitude  $\Delta n$  is always the same at  $E_{(\eta_{\text{max}})}$  (over-modulation field). The latter can, therefore, be regarded as a convenient parameter characterizing the PR performance of a material [17]: the lower  $E_{(\eta_{\text{max}})}$  for a given composite, the higher is  $\Delta n$  at any given external field and the better is its PR performance.

The PR two-beam coupling (TBC) gain  $\Gamma$  was calculated according to [15]

$$\begin{aligned} \Gamma = \frac{1}{d} & \left[ \cos \alpha_{1,\text{int}} \ln \left( \frac{I_1(E)}{I_1(E=0)} \right) \right. \\ & \left. - \cos \alpha_{2,\text{int}} \ln \left( \frac{I_2(E)}{I_2(E=0)} \right) \right], \end{aligned} \quad (3)$$

where  $\alpha_{1(2),\text{int}}$  are the angles of the writing beams with regard to the sample normal measured inside the material,  $I_{1,2}(E)$  are the intensities of the writing beams behind the sample at some applied electric field  $E$ , and  $d$  is the thickness of the active layer.

The field-dependent steady-state data were determined by gradually increasing the applied voltage in steps of 250 V. To allow the systems to reach quasi-steady-state conditions, the data were taken with a 90 s time interval between each step. For the dynamic measurements, the samples were illuminated by the 1 writing beam for 600 s without an electric field applied. Then the devices were poled for 120 s by applying an electric field of  $E = 43\text{ V }\mu\text{m}^{-1}$ . During that time, which was sufficiently long enough to reach the quasi-steady state for poling, the sample was illuminated uniformly by beam 1. To start the recording, a magnetic shutter switched the second writing beam on. Data collection started 10 ms prior to the switching. The recording process is rather complicated (e.g., space-charge field formation and chromophore orientation take place simultaneously), and thus throughout the following discussion the time necessary to achieve 50% of the quasi-steady-state diffraction efficiency (measured after 300 s),  $\tau_{50}^r$ , was chosen as a phenomenological metric of comparison for the recording data. Similarly, the time necessary to erase the gratings by the writing beam 2 to 50% of their previous strength,  $\tau_{50}^e$ , will be quoted.

### 3 Experimental results

#### 3.1 Photo-current measurements

The electric field dependences of the photo-current amplitude  $j_{\text{ph}}^\Omega$  are depicted in Fig. 2 for selected materials (R/A/C/I and R'/A'/C'/I', respectively). The plots for the other samples with intermediate concentrations of NP are in between—showing all data would overload Fig. 2. We found that the field dependence of  $j_{\text{ph}}^\Omega$  is super-linear in all cases, indicating geminate recombination typical for polymeric photo-conductors [18, 19]. The photo-current amplitude  $j_{\text{ph}}^\Omega$  increases sub-linearly with the LiNbO<sub>3</sub> content and is more than one order of magnitude larger for the materials containing TNF than for those without TNF at identical LiNbO<sub>3</sub> content. This is expected since TNF is the sensitizer commonly used with PVK [4–6]. In the reference material R' we find that  $j_{\text{ph}}^\Omega$  does not vanish, i.e., charge generation processes take place even in the absence of TNF. Furthermore, a sample which contains only PVK and LiNbO<sub>3</sub> NP (without chromophores and without TNF) does not exhibit any photo-current (not shown).

#### 3.2 Steady-state PR performance

The PR properties of the two series of materials show a similar dependence of the steady-state PR performance on the

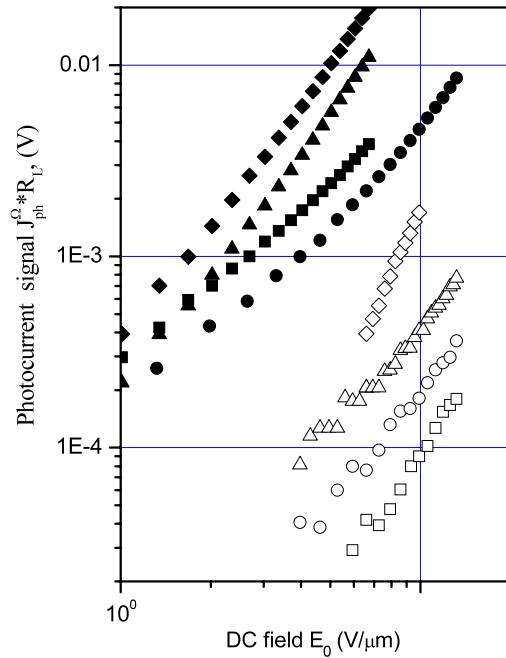


**Fig. 2** External-DC-field dependence of the photo-current signal for different concentrations of  $\text{LiNbO}_3$  nano-particles: material R (solid squares), material A (solid circles), material C (solid triangles), and material I (solid rhombus); material R' (open squares), material A' (open circles), material C' (open triangles), and material I' (open rhombus)

NP content both for DFWM and TBC. Figure 3a presents the field strength necessary to reach the electric field for over-modulation of the diffraction,  $E_{(\eta \max)}$ , as a function of the  $\text{LiNbO}_3$  nano-particle concentration. For comparison,  $E_{(\eta \max)}$  of the reference material R is indicated by a solid line. The second reference material R' did not show any photo-refractivity under the conditions described earlier in the article (can be seen only on much longer time scales [20, 21]). For the materials containing TNF (A–I),  $E_{(\eta \max)}$  is generally smaller by about 10 V/ $\mu\text{m}$  than for the materials without TNF, but identical  $\text{LiNbO}_3$  content (A'–I'). Within one series, the best PR performance (lowest  $E_{(\eta \max)}$ ) has been obtained with the material sensitized with  $10^{-3}$  wt.%  $\text{LiNbO}_3$  (C and C'). In both series the best material is superior to the reference material (R and R'), respectively.

Figure 3b shows the dependence of the TBC gain coefficient  $\Gamma_s$  on the  $\text{LiNbO}_3$  nano-particle concentration. The DC-field value that corresponds to maximum diffraction in the best material C ( $47.25 \text{ V } \mu\text{m}^{-1}$ ) was selected for comparison purposes. The gain reaches the highest values at a  $\text{LiNbO}_3$  content of  $10^{-3}$  wt.%. For the materials, sensitized with  $\text{LiNbO}_3$  only (A–I), the gain is consistently larger than in the material co-sensitized with TNF (A'–I'). Since the opposite holds for the index modulation  $\Delta n$  (it is larger in the series A–I as compared to series A'–I'), we conclude that the photo-refractive phase shift is reduced in the materials

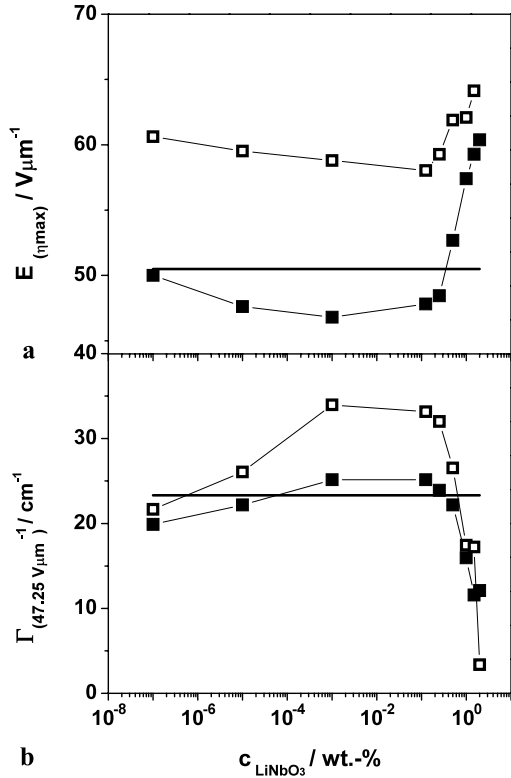


**Fig. 3** Dependence of the field of maximum diffraction in DFWM experiments  $E_{(\eta \max)}$  (a) and the gain coefficient for s-polarized beams  $\Gamma_s$  measured at  $47.25 \text{ V } \mu\text{m}^{-1}$  (b) on the concentration of  $\text{LiNbO}_3$  nano-particles: materials sensitized with TNF and  $\text{LiNbO}_3$  (A–I, solid symbols), materials sensitized with  $\text{LiNbO}_3$  only (A'–I', open symbols). The thick solid lines indicate the performance of the reference material R. All other lines are guides to the eye

containing TNF (A–I) as compared with the series without TNF (series A'–I').

### 3.3 Dynamic PR performance

The time-resolved diffraction efficiencies upon recording and erasure were measured according to the scheme described in the experimental section. The results are shown in Fig. 4. Both recording and erasure are faster by about one order of magnitude in the materials sensitized with TNF (A–I) compared to those not containing TNF (A'–I'). In both groups of materials erasure is faster than recording by a factor of 2–3. The recording/erasure speed is only slightly affected by changes of the NP content; the variations within one series of materials are less than a factor of 2.

## 4 Discussion

Our experimental data allow drawing conclusions about the role of  $\text{LiNbO}_3$  NP on space-charge formation in this hybrid material. Here, we put forward a scheme explaining the

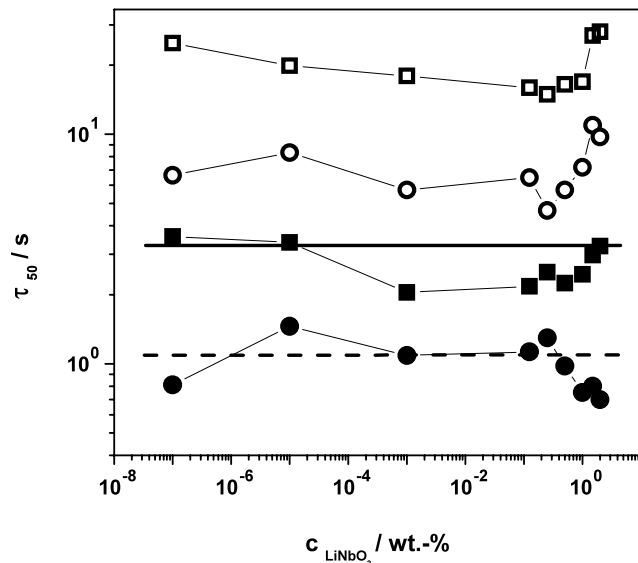


**Fig. 4** Holographic response times during recording  $\tau_{50}^r$  (squares) and erasure  $\tau_{50}^e$  (circles) for the materials sensitized with TNF and LiNbO<sub>3</sub> (A–I, solid symbols) and materials sensitized with LiNbO<sub>3</sub> only (A'–I', open symbols) obtained at  $43 \text{ V } \mu\text{m}^{-1}$ . The thick solid (dashed) line indicates  $\tau_{50}^r$  ( $\tau_{50}^e$ ) for the reference material R

energetic situation (Fig. 5). Our previous results indicated that the LiNbO<sub>3</sub> conduction band (CB) edge lies below the lowest unoccupied molecular orbital (LUMO) level of the sensitizer (TNF and/or chromophore) [13]. Absorption of a photon catapults an electron from the highest occupied molecular orbital (HOMO) of the sensitizer to the LUMO, followed by an electron transfer to the LiNbO<sub>3</sub> CB. Due to its size (20 nm in diameter) one particle can host several charges, thus, will act as a multi-electron trap. Accumulation of charges eventually leads to band bending and creation of recombination barriers (formation of potential wells), which hinder recombination with holes (Fig. 5, right). This will ultimately reduce the probability of geminate recombination and, thus, improve charge generation and transport. Thus LiNbO<sub>3</sub> NPs by themselves do not contribute to charge generation but they seem to enhance the photo-conductivity.

Now we check whether this model is capable of explaining our experimental observations. TNF and LiNbO<sub>3</sub> NP of sufficient concentration, they both enlarge the photo-conductivity, as it is evident from Fig. 2. The model described above, stating that LiNbO<sub>3</sub> NP are very effective traps for electrons and hence increase the production of holes, easily explains the NP-induced increase of the conductivity. Charge generation probably takes place via light absorption by the PVK/TNF charge-transfer complex (materials A–I and R only) and by the chromophores (DMN-PAA/MNPAA) [22].

There is almost no influence of the NP on the steady-state over-modulation field (Fig. 3a), up to a threshold concentration of  $10^{-3}$  wt.%. However, in the same range of con-

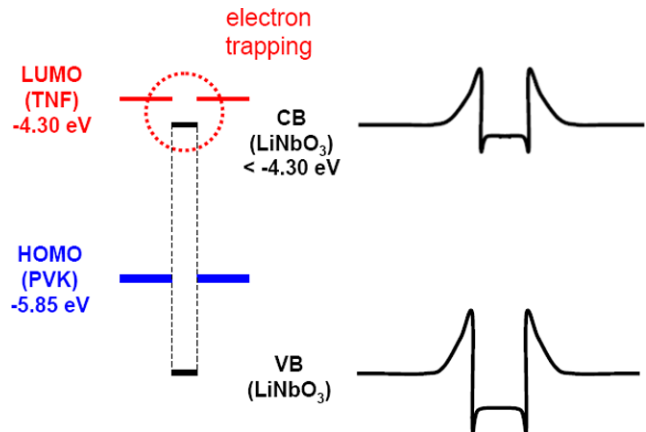


**Fig. 5** Energy scheme of the PR composite containing LiNbO<sub>3</sub> NP. The band-bending effect and creation of the drift and recombination barriers is illustrated on the right

centrations we observe a pronounced increase of the TBC (Fig. 3b). Since the amplitude of the PR index modulation is almost unchanged, this must be attributed to a larger phase shift between index and light patterns. Larger transport lengths can explain this effect; again in accordance with the model explained earlier in the text that predicts improved hole transport [13]. Addition of TNF increases the photo-conductivity as well but by putting more charge carriers into the system and not by increasing the transport lengths, thus leaving the TBC at smaller values.

Above LiNbO<sub>3</sub> NP contents of about  $10^{-3}$  wt.%, the PR performance deteriorates with increasing NP content (Fig. 3). There are two reasons for this: first, for a NP content of about 1 wt.% the average separation distance  $l$  between particles becomes comparable to the Debye screening length ( $l \approx r_D$ ) [13], thus, the space-charge field collapses because now almost all mobile holes generated in the volume of the composite are participating in screening of the charges trapped inside the nano-particles, so there is no net charge separation which is necessary for observation of the photo-refractive effect. Second, the optical quality of the composite is diminished, i.e., light scattering increases.

Figure 4 reveals almost no dependence of the response time on the LiNbO<sub>3</sub> NP concentration. This is somehow surprising, since Fig. 2 clearly shows an increase of the photo-conductivity by the addition of LiNbO<sub>3</sub> NP. Here one has to consider that Fig. 2 shows the AC conductivity at a modulation frequency of 10 Hz, while Fig. 4 shows time constants of the order of 1–20 s. Thus the AC conductivity—where charge generation has a strong impact—is clearly influenced by the LiNbO<sub>3</sub> NP. The DC conductivity relevant for the dynamics of DFWM and TBC is obviously much less influenced by charge generation—there the LiNbO<sub>3</sub> NP influence mainly the transport length.

## 5 Conclusions

The aim of this work was the first study of a new class of hybrid materials, combining two of the most studied photorefractive systems. In DFWM and TBC experiments the PR properties of materials based on PVK sensitized with LiNbO<sub>3</sub> NP and TNF as well as with LiNbO<sub>3</sub> NP alone were studied and compared with those of the standard material sensitized with TNF. Photo-current and photo-refractive parameters were studied as a function of the LiNbO<sub>3</sub> NP concentration.

An impact of the LiNbO<sub>3</sub> NP is seen even for extremely low concentrations of 10<sup>-7</sup> wt.%. We observed that in composites with low concentration of nano-particles (from 10<sup>-7</sup> to 10<sup>-3</sup> wt.%) the PR performance increases with the content of LiNbO<sub>3</sub>. The optimum is reached at 10<sup>-3</sup> wt.% LiNbO<sub>3</sub>. For higher contents of NP (from 10<sup>-1</sup> to 5 wt.%) the performance gradually worsens. We attribute this finding to Debye screening and light scattering due to aggregation of the nano-particles.

**Acknowledgements** The authors thank Elisabeth Soergel and Konrad Peithmann (University of Bonn) for helpful discussions. Dr. S. Mansurova thanks the Alexander von Humboldt Foundation for the financial support. Financial support by the German Research Foundation (DFG), European Space Agency (ESA), and the Deutsche Telekom AG is also gratefully acknowledged.

## References

1. A. Ashkin, G.D. Boyd, J.M. Dziedzic, R.G. Smith, A.A. Ballman, J.J. Levinstein, K. Nassau, *Appl. Phys. Lett.* **9**, 72 (1966)
2. P. Günter, J.-P. Huignard, *Photorefractive Materials and Their Applications*. Topics in Applied Physics, vol. 62 (Springer, Berlin, 1988)
3. S. Ducharme, J.C. Scott, R.J. Twieg, W.E. Moerner, *Phys. Rev. Lett.* **66**, 1846 (1991)
4. K. Meerholz, B.J. Volodin, Sandalphon, B. Kippelen, N. Peyghambarian, *Nature* **371**, 497 (1994)
5. K. Meerholz, *Angew. Chem.* **36**, 945 (1997)
6. K. Meerholz, B. Kippelen, N. Peyghambarian, in *Electrical and Optical Polymer Systems*, ed. by D.L. Wise, G.E. Wnek, D.J. Trantolo, J.D. Gresser, T.M. Cooper (World Scientific, Singapore, 1998)
7. W.E. Moerner, A. Grunnet-Jepsen, C.L. Thompson, *Annu. Rev. Mater. Sci.* **27**, 585 (1997)
8. O. Ostroverkhova, W.E. Moerner, *Chem. Rev.* **104**, 3367 (2004)
9. J.G. Winiarz, L. Zhang, M. Lal, C.S. Friend, P.N. Prasad, *Chem. Phys.* **245**, 417 (1999)
10. J.G. Winiarz, L. Zhang, M. Lal, C.S. Friend, P.N. Prasad, *J. Am. Chem. Soc.* **121**, 5287 (1999)
11. K.R. Choudhury, J.G. Winiarz, M. Samoc, P.N. Prasad, *Appl. Phys. Lett.* **82**, 406 (2003)
12. K. Meerholz, Y. de Nardin, R. Bittner, *Mol. Cryst. Liq. Cryst.* **315**, 99 (1998)
13. S. Mansurova, U. Hartwig, E. Śliwińska, K. Buse, K. Meerholz, Enhancement of the charge carrier transport by doping PVK-based photoconductive polymers with LiNbO<sub>3</sub> nano-sized crystals. *Phys. Rev. B* (accepted)
14. J.R. Schwesig, H.A. Eggert, K. Buse, E. Śliwińska, S. Khalil, M. Kaiser, K. Meerholz, *Appl. Phys. B* **89**, 15 (2007)
15. K. Meerholz, B. Kippelen, N. Peyghambarian, in *Photonic Polymer Systems* (Dekker, New York, 1998)
16. H. Kogelnik, *Bell Syst. Tech. J.* **48**, 2909 (1969)
17. R. Bittner, T.K. Däubler, D. Neher, K. Meerholz, *Adv. Mater.* **11**, 123 (1999)
18. P.M. Borsenberger, D. Weiss, *Organic Photoreceptors for Xerophotography* (Dekker, New York, 1998)
19. H. Bässler, Semiconducting and photoconducting organic solids, in *Organic Molecular Solids: Properties and Applications*, ed. by W. Jones (CRC Press, New York, 1997)
20. E. Mecher, F. Gallego-Gómez, H. Tillmann, H.H. Hörlold, J.C. Hummelen, K. Meerholz, *Nature* **418**, 959 (2002)
21. E. Mecher, F. Gallego-Gómez, H. Tillmann, H.H. Hörlold, J.C. Hummelen, K. Meerholz, *Chem. Phys. Chem.* **5**, 277 (2004)
22. M. Salvador, F. Gallego-Gómez, K. Meerholz, *Appl. Phys. Lett.* **90**, 154102 (2007)